EOF Analysis of Central Drake Passage Currents from DRAKE 79

JOHN M. KLINCK

Department of Oceanography, Texas A&M University, College Station, TX 77843

(Manuscript received 9 September 1984, in final form 7 December 1984)

ABSTRACT

A rotary Empirical Orthogonal Function analysis was performed on the current meter observations made during DRAKE 79 to quantify current variability in central Drake Passage in the vicinity of the Polar Front. Two forms of variability are revealed by the analysis: a large scale north–south shift of the Polar Front and meandering of the Polar Front. The frontal shift influences the current at the three nominal observation levels (500 m, 1400 m, 2500 m) over most of the central passage, with a time scale of about three months. Variability associated with meanders (also warm-core and cold-core rings) extends over the whole central passage. Currents as far south as ML-10 are influenced by rings that pass by the northern side of the MS array. These events occur at somewhat regular intervals of one and a half to two months.

This analysis shows that the rugged bottom topography in the central part of Drake Passage plays a dominant role in the variability of the currents. Additionally, the strong current associated with the Polar Front tends to flow around the seamounts located in the central passage. Steering also affects the cold-core rings which travel through the region.

1. Introduction

The International Southern Ocean Studies (ISOS) included a five-year project to study the Antarctic Circumpolar Current (ACC) as it flows through Drake Passage. A series of preliminary current meter deployments, beginning in 1975, addressed certain aspects of the flow in Drake Passage, such as lateral coherence scales and variability in the vicinity of the Polar Front. The preliminary current meter deployments were used to design a year-long (1979–80) measurement program which spanned the whole passage.

The current meter array for this year-long experiment (DRAKE 79) consisted of two major parts (Fig. 1a, b). The main line (ML) array was designed to measure the total transport through the passage and a cluster of moorings in the central passage constituted a mapping and statistics (MS) array which sampled the flow variability in the Polar Frontal Zone. Current meters were positioned at nominal depths of 500 m and 2500 m on all moorings and at 1400 m on the MS moorings; the actual depths were sometimes more than 100 m different from the nominal values (see Pillsbury *et al.*, 1981).

The MS moorings are located in the central passage where the bottom bathymetry is quite rugged (Fig. 1b), with a line of seamounts, stretching roughly north-south between longitudes 65°W and 66°W. The DRAKE 79 current observations as discussed in this study and Hofmann and Whitworth. (1985) indicate that bottom topography plays an important role in the flow variability that is observed in this region.

As a result of the ISOS program we know that the general structure of the flow in Drake Passage, most recently studied by Nowlin *et al.* (1977), Whitworth (1980) and Nowlin and Clifford (1982), consists of three fronts supporting strong, baroclinic currents. The zones between the fronts have relatively uniform properties and generally sluggish flow.

The Polar Frontal Zone, between the Subantarctic Front and the Polar Front, is generally located in the north-central part of the passage (near 59°S) but its position is subject to considerable variability (Whitworth, 1980). The flow in the Polar Frontal Zone is quite dynamic; both meanders and rings have been observed (Legeckis, 1977; Joyce and Patterson, 1977; Joyce *et al.*, 1981; Peterson *et al.*, 1982). Furthermore, calculations by Bryden (1979) show the flow in the Polar Front to be baroclinically unstable, as one might expect given the strongly sloping isopycnals in the fronts. This instability provides a dynamic mechanism to create meanders and rings.

Sciremammano *et al.* (1980) analyzed the lateral coherence of currents measured during 1975, 1976 and 1977 in an attempt to identify the lateral scales of the flow. They found that lateral correlation scales for velocity in the central passage were quite short (30 to 80 km), generally being shorter in the transverse than in the longitudinal direction and about the correct size for rings and meanders. These short scales

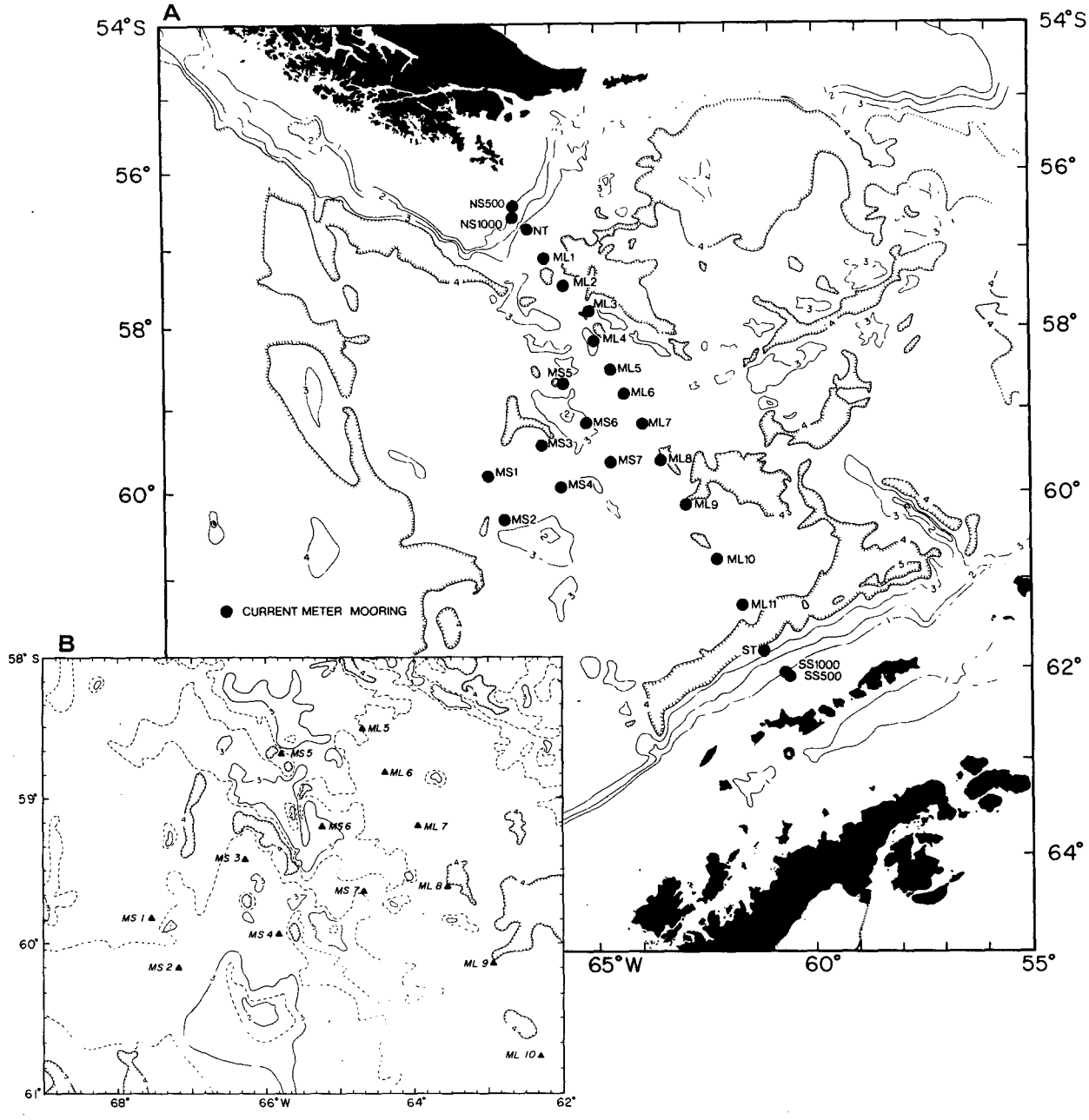

FIG. 1. (a) Drake passage and the general location of DRAKE 79 current moorings. (b) Locations of moorings used in this study. Depth contours are shown at 1000 m intervals with the dashed contours showing 500 m depths.

further indicate that the ACC in central Drake Passage is not a broad, coherent current but is composed of narrow frontal jets and mesoscale rings.

An extensive analysis of all of the current measurements from ISOS (Inoue, 1982) reveals a relatively simple vertical structure. The flow tends to be composed of a barotropic and first baroclinic mode, with surface velocities larger, in general, than bottom velocities. Only one mooring (MS-5) displayed pronounced bottom intensified motion which seems to be due to this mooring's location in a gap between two seamounts (Fig. 1b). The question of bottom steering of the currents will be considered at the end of this paper.

A study of the variability of the currents revealed by the DRAKE 79 observations has been pursued by Hofmann and Whitworth (1985). From this study we find that variability of the currents in central

Drake Passage takes the form of lateral (up to 100 km) shifts of the Polar Front, meandering of the Subantarctic and Polar Fronts and passage of cold- and warm-core rings through the array. There is one case where a meander may have formed a cold-core ring within the MS array.

The purpose of the present study is to analyze the flow in the central part of Drake Passage from the DRAKE 79 measurements. Specifically, features of the flow will be separated and the energy (or variance) of these features quantified. The spacing of the moorings is adequate (40 to 80 km) to detect the individual features that cause variability in the current. It is also possible to estimate the frequency of the events and to determine temporal and spatial relationships among them.

The major tool in this analysis is complex (or rotary) Empirical Orthogonal Function (EOF) analysis, also known as Principle Component analysis (for a general description see Priesendorfer *et al.*, 1981). Complex here implies that the two-dimensional velocity observations are taken to be complex quantities, thereby preserving vector information. Rotary EOF analysis allows differentiation of current variations as direction changes or as magnitude changes. The utility of EOF analysis is that a small number of patterns may explain most of the variability in a data set. Furthermore, energetic events with different temporal structure should appear in different EOF modes, i.e., patterns of variability can be separated.

Section 2 outlines the construction of EOF modes and amplitude series and presents the particulars of the DRAKE 79 data set. Several exploratory analyses are mentioned which consider how the results differ with different numbers of sensors or different lengths of time series. Section 3 presents the analysis of the longest time series that can be extracted from the DRAKE 79 measurements. Section 4 interprets the EOFs and their variability in terms of dynamical features, mainly rings, meanders and frontal shifts as well as the influence of bottom topography.

2. Methods

a. EOF analysis

Empirical Orthogonal Function analysis on scalar time series is discussed in Priesendorfer *et al.* (1981) along with a mechanical analog for the analysis, and a catalog of the past users of EOF analysis. Extensions of the scalar analysis to two-dimensional vector (complex) time series is straightforward (Hardy, 1977; Hardy and Walton, 1978, Denbo and Allen, 1984). The following outline of complex EOF analysis uses the notation of Legler (1983).

We define the data under consideration as

$$\mathbf{W}_{jk} = (u_{jk} - \overline{u_k}) + \sqrt{-1}\,(v_{jk} - \overline{v_k}),$$

where u and v are eastward and northward components of velocity and the overbars indicate a time average. The index j is a time counter from 1 to N, where N is the total number of measurements in the time series, and k is a sensor index in the range 1 to M, where M is the total number of sensors. The matrix $\mathbf{W}$ is then $N \times M$ and is composed of complex numbers representing the zero mean velocity data set.

A $M \times M$ covariance matrix is defined as

$$\mathbf{H} = \frac{1}{N}\mathbf{W}\mathbf{W}^{\mathrm{T}},$$

where the T superscript denotes complex conjugate transpose. The matrix $\mathbf{H}$ is hermitian, i.e., it is equal to the conjugate transpose of itself. This guarantees that the eigenvalues of the matrix will be real.

The essence of EOF analysis is that the covariance matrix is partitioned into a set of eigenfunctions which are mutually orthogonal. That is,

$$\mathbf{H}\mathbf{e}_m = \lambda_m \mathbf{e}_m,$$

where $\mathbf{e}_m$ is the eigenvector and

$$\mathbf{e}_m \cdot \mathbf{e}_n^* = \delta_{mn}$$

where the asterisk denotes the complex conjugate.

Furthermore,

$$\mathrm{TRACE}\,(\mathbf{H}) = \sum_m \lambda_m = \text{total variance of the data set.}$$

Therefore, the magnitude of an eigenvalue indicates the percentage of the total variance explained by that eigenvector. In this case, the eigenvectors are spatial patterns of velocity (represented by a complex number) at the various current meters.

The eigenvectors form a complete and orthogonal basis for the data matrix $\mathbf{W}$ so it can be expanded in terms of $\mathbf{e}_m$ as

$$[\mathbf{W}]_{jk} = \sum_m A_{jm}[\mathbf{e}_m]_k,$$

where A_{jm} is a time series (j = 1 to N) of amplitudes for the mth EOF. This converts the data set from a set of individual time series to a set of spatial patterns that vary in time.

The principal question in this sort of analysis is which EOF modes are meaningful. Priesendorfer *et al.* (1981) discuss selection rules for EOFs. They recommend a combination of two rules to determine which modes are nonrandom. One rule tests if eigenvalues are significantly different from a random expected value. The other rule is based on a Monte Carlo calculation where random normal values define a data set. Many evaluations of random data give range of eigenvalues for purely random data. Eigenvalues from the actual observations that depart from

this pattern are taken to be meaningful. The larger result from both tests is taken to be the number of significant modes. The reader is referred to Priesendorfer *et al.* (1981) for details on these and other EOF selection rules.

b. Current meter data

The central passage current meter data from DRAKE 79 are summarized in Table 1. (For details of the whole DRAKE 79 data set, see Pillsbury *et al.*, 1981). Since low frequency current variations are analyzed, 40-hour low-pass filtered time series, sampled daily, are used. The depth indications are nominal; the actual depths vary considerably from these values (Pillsbury *et al.*, 1981). The nominal depths provide a reasonable partition of the current observation into three general depth categories.

Thirty-three current meters in the central passage returned usable data. Continuous data are available for the first 123 days after which some sensors ceased working or yielded unreliable observations. Other subsets of the data are obtained by excluding shorter time series. These subsets allow analysis of 275 days of data at 31 sensors, 300 days at 30 sensors, 325 days at 29 sensors or 352 days at 27 sensors. An EOF analysis was performed on each of these subsets. The results were all similar (except the 352 day subset). This similarity occurs because the currents on the northern side of the array at 500 m (ML5, ML6, ML7, MS5) have the largest variance and therefore dominate the analysis. As long as these sensors are included in the analysis, the results will be similar.

The longest analysis considered is that of 29 sensors for 325 days (see Table 2 for details). A test for the number of significant EOFs, based on the selection rules of Priesendorfer *et al.* (1981), reveals that the first five EOF modes are nonrandom (Fig. 2). The following analysis will consider only these five modes. One longer analysis is possible with 352 days of data but it would exclude mooring ML-7 at 500 m which has the second largest variance of the entire dataset. Thus, excluding this mooring from the analysis yields a rather different partition of variance.

TABLE 1. 40 h low-pass data available from the central Drake Passage moorings from DRAKE 79. The numbers in the table give the Julian days for which current observations are available. Day 1 is 1 January 1979. The depth columns are nominal depths; actual sensor depths may vary from these nominal values.

Mooring	500 m	1400 m	2500 m
ML-5	34–388	31–385	31–358
ML-6	34–388	31–385	31–385
ML-7	34–361	31–385	31–385
ML-8	34–333	no data	no data
ML-9	34–388	no data	31–385
ML-10	34–388	no data	31–385
MS-1	34–185, 225–333 367–385	31–385	31–385
MS-2	34–385	31–385	31–385
MS-3	34–387	no data	no data
MS-4	34–156, 293–386	31–385	31–385
MS-5	34–388	31–385	31–385
MS-6	34–388	31–385	31–385
MS-7	34–385	31–385	31–308

TABLE 2. Detail of the analysis with 29 sensors and 325 days of data. The time series span day 34 to 358 (3 February 1979 to 24 December 1979).

Nominal depth	Sensors included
500 m	ML-5, ML-6, ML-7, ML-9, ML-10 MS-2, MS-3, MS-5, MS-6, MS-7
1400 m	ML-5, ML-6, ML-7 MS-1, MS-2, MS-4, MS-5, MS-6, MS-7
2500 m	ML-5, ML-6, ML-7, ML-9, ML-10 MS-1, MS-2, MS-4, MS-5, MS-6

3. Results

Before attempting to interpret the EOFs in terms of physical phenomena, it is necessary to determine which EOF modes contain variability from which current meter records. The five significant EOF modes and the mean velocities are used to reconstruct the velocity observations. The subtraction of the recon-

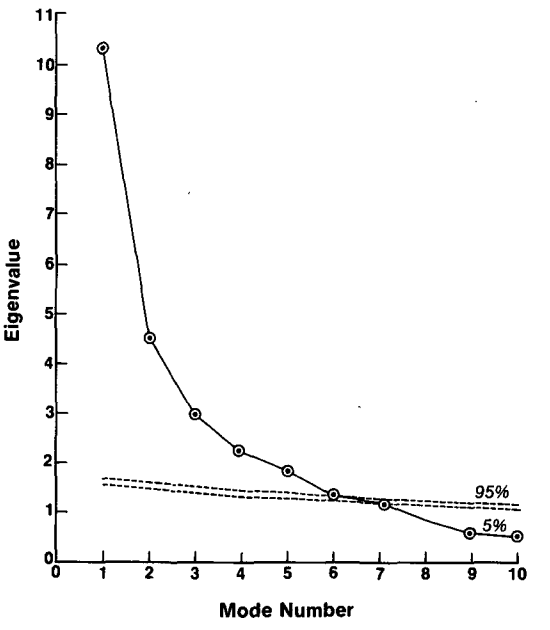

FIG. 2. Eigenvalues (normalized by the mean variance of the data set) from the EOF analysis with 29 sensors for 325 days are shown in solid symbols. The dashed lines indicate the 5th and 95th percentile eigenvalues from a Monte Carlo experiment (100 trials, with unit normal random observations). The first five eigenvalues are significant.

structed and original velocity time series yields a residual series, the variance of which indicates how well a given EOF mode explains variance at a given sensor.

Table 3 presents the residual variance for the mode by mode reconstruction of the velocity observations. Only those sensors (17 out of 29) are listed for which more than 20% of the variance is explained by all five modes.

This choice is somewhat arbitrary but reconstruction of the times series of velocity at these ignored sensors is not very different from the mean and bears little resemblence to the original time series. The implication of this fact is that these sensors are not strongly associated with the dynamic activity represented by the modes. Inclusion of these sensors in the table would add no additional information.

The results of the residual variance calculation are summarized on Fig. 3 which displays the time mean vectors for all sensors. Below each meter location is the variance of the data; the superscripts on these numbers are the EOF modes which reduce the residual variance by more than 20%.

There is a general pattern to the distribution of important modes. The first mode fits variance on the northern side of the array (ML-5, ML-6), generally at all levels, while the second mode explains variability from ML-5, ML-6, ML-7. The third mode represents mainly MS-5 in the upper levels. The fourth and fifth modes explain variance in the southern part of the array.

For some sensors there is a general decline in the variance for each mode without a strong reduction for a given mode (e.g., MS-2). Such cases have less than 25% of the total variance explained by all modes and will not be given much consideration in the analysis.

The time mean currents (Fig. 3) provide a current spatial pattern, the departure from which provides the variance. The mean currents are generally through passage (50°T). At MS-1 and MS-2, the mean current is generally to the north reflecting the presence of a sea mount at 60.5°S, 66°W (Fig. 1b). The current at MS-5, 2500 m is along the axis of a deep valley (Fig. 1b). The southern moorings (ML-9, ML-10) have mainly across passage mean flow reflecting the presence of a downsteam submerged ridge (59°S, 59°W to 61°S, 57°W) which blocks the flow (Reid and Nowlin, 1971).

The time variation of the EOF modes relates to activity at certain meters as revealed by the variance calculation. Some interpretation of the current variations is possible from the amplitude series. A lagged correlation analysis of these time series is considered to quantify time scales of the modes and the temporal associations among them.

The time dependent amplitudes for each of the five modes are shown in Fig. 4a–e. The variance

TABLE 3. Analysis of the variance ($cm^2\ s^{-2}$) explained by the EOFs. The second column is the original variance. The columns in the table are the residual variance after subtracting the reconstructed velocity from the original data. The final column is the percentage of the total variance explained by all five of the significant modes. Only those sensors are listed for which at least 20% of the total variance is explained by all five modes.

Mooring	Total variance	Residual variance after fitting EOFs					Variance explained
		1	2	3	4	5	
500 m							
ML-5	233.3	63.8	24.3	21.2	20.3	17.4	92%
ML-6	152.5	85.4	43.6	36.9	39.5	37.8	75%
ML-7	160.9	178.9	95.9	70.6	40.0	35.8	78%
ML-10	84.7	87.7	87.3	87.2	48.5	25.6	70%
MS-2	53.5	48.9	48.7	42.1	40.2	40.6	24%
MS-5	136.9	113.7	97.3	28.4	29.9	30.4	78%
MS-7	83.0	82.9	75.7	61.7	42.5	39.9	52%
1400 m							
ML-5	72.6	23.3	13.6	11.8	12.5	10.9	85%
ML-6	49.8	28.0	18.9	18.3	21.1	21.2	57%
ML-7	43.2	49.9	29.6	21.5	13.0	11.5	73%
MS-2	14.6	13.5	13.5	12.0	11.6	11.6	21%
MS-5	40.6	34.5	28.0	10.1	9.5	8.4	79%
MS-6	35.1	29.2	31.9	33.9	31.1	26.1	25%
MS-7	25.8	27.3	25.3	20.6	14.3	13.9	46%
2500 m							
ML-5	30.0	22.2	21.5	21.2	21.6	21.7	28%
ML-7	20.3	24.6	19.7	17.8	16.4	16.1	21%
ML-9	24.5	24.5	25.1	25.8	18.3	11.2	54%

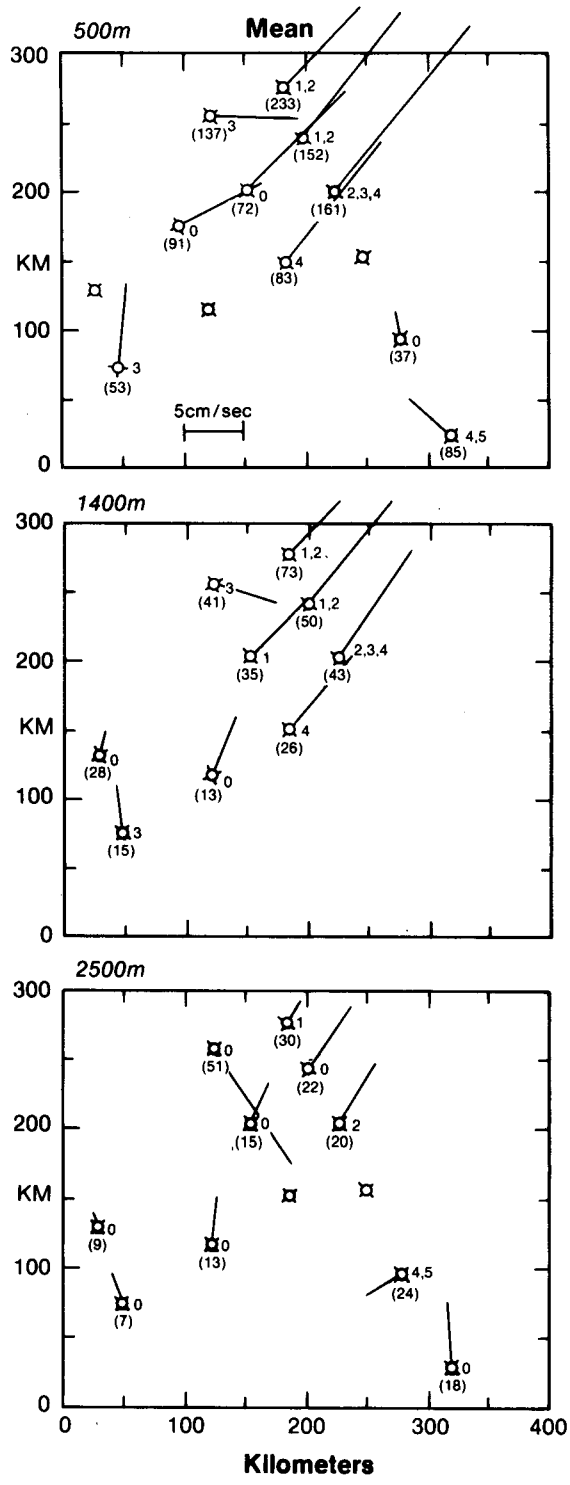

FIG. 3. Mean velocity vectors from the 29 sensor, 325 day analysis. The circles indicate the current meter locations. The number in parenthesis at each current meter is the variance (cm^2 s^{-2}) for that sensor. The superscripts on the variance show which EOF modes explain 20% or more of the residual variance. A zero indicates that less than 20% of the total variance of the sensor is explained by all five EOF modes.

calculation indicates that these amplitude series apply to one or, at most, a few current meters, so the direction is taken to be the current direction for the important meter(s). The EOF spatial structure is shown in Fig. 5a–e. Recall that the total velocity is obtained by adding the mean velocity vectors to the EOF vectors (product of spatial structure and complex amplitude).

The first mode amplitude series (Fig. 4a), which applies mainly to the velocity at ML-5 at 500 m, has a relatively simple structure. The direction maintains one of two states—north or southwest—despite magnitude changes. Northward velocities add to the mean at ML-5 (Fig. 3) and are associated with high speed flow on the northern side of the array. A southwestward vector cancels part of the mean resulting in slower flow at ML-5.

Three changes stand out in mode one. There is a rapid change of direction between days 85 and 90 (26–31 March), which occurs at a minimum in amplitude. The transition from one state to the other occurs over a longer time from day 75 (16 March) to day 95 (5 April). The second change is a return to a northward direction that takes place from day 185 (4 July) to day 210 (29 July). This transition is not associated with a clear minimum in magnitude as was the first event. There is a third direction change from day 285 (12 October) to day 315 (11 November), again not clearly associated with a magnitude minimum. This last change is a rotation of the current from northward in a counterclockwise direction back to northward.

The interpretation of this pattern is that a fast current, that associated with the Polar Front, is near ML-5 from January until late March when it shifts to the south. The strong current returns to ML-5 near the end of July. The last event is a 30-day rotation of the current which is associated with a short-lived southward shift of the front.

The EOF mode 2 (Fig. 4b) has a rather different temporal structure and is associated with ML-5 at 500 m and with ML-6 and ML-7 at 500 m to some extent. The amplitude has a repetitive behavior with relatively constant plateaus in strength separated by times of zero magnitude, which occur every 50 to 60 days. The implication of this behavior is that these are the rings and meanders of the Polar Front that have been observed in central Drake Passage (e.g., Peterson *et al.*, 1982). Further support that these are rings is seen in the direction series which shows clockwise (cyclonic) rotation of velocity vectors during maxima in magnitude.

There is some correspondence of the behavior of EOF 2 with the state of EOF 1. The three events between days 90 and 210 (times when the front is to the south) have a turning of the current from east to south to west, which is consistent with a cyclonic

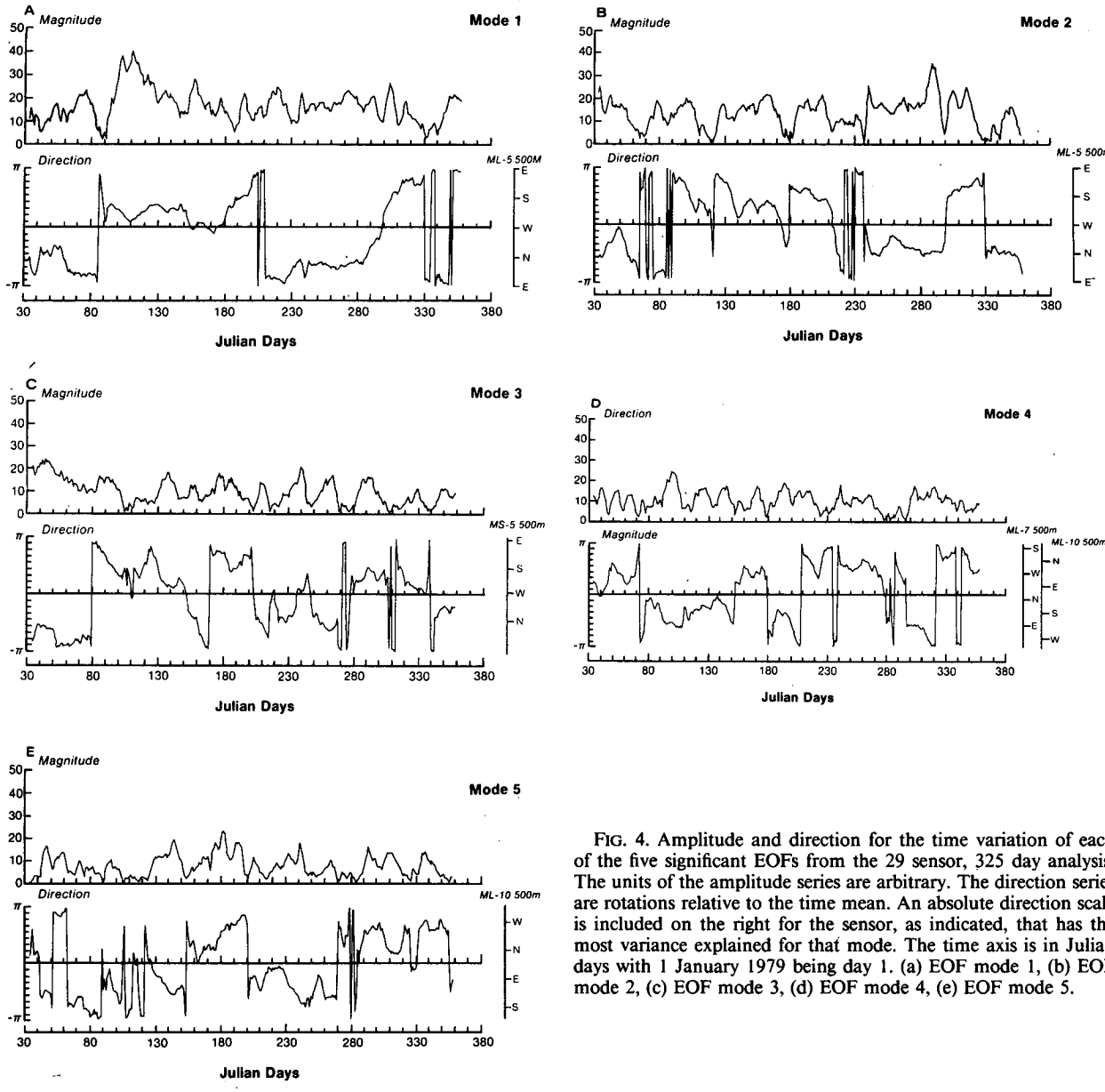

FIG. 4. Amplitude and direction for the time variation of each of the five significant EOFs from the 29 sensor, 325 day analysis. The units of the amplitude series are arbitrary. The direction series are rotations relative to the time mean. An absolute direction scale is included on the right for the sensor, as indicated, that has the most variance explained for that mode. The time axis is in Julian days with 1 January 1979 being day 1. (a) EOF mode 1, (b) EOF mode 2, (c) EOF mode 3, (d) EOF mode 4, (e) EOF mode 5.

ring passing north of ML-5. For the period between days 30 and 80 and days 210 and 280 (when the Polar Front is near ML-5), the current change is from north to west to north. For these times, the ring only slows the current at ML-5 rather than causing a full turning of the velocity.

The transition at day 300 (27 October) turns in the opposite direction from the others—north to west to south—which is a counterclockwise rotating, usually associated with "warm core" mesoscale features. This rotation is followed by a clockwise ("cold core") rotation which is likely a following meander.

The EOF mode 3 (Fig. 4c) explains the most variance at MS-5 at 500 m and 1400 m. The temporal character of the time series is quite like that of EOF 2 in that there are many times when the amplitude attains about the same value and these times are associated with direction changes. This EOF mode represents the current changes at MS-5 due to rings and meanders on the northern side of the array. The direction of rotation for the times of high magnitude is first one way, then the other. This behavior reflects the fact that in this region, cyclonic rings are associated with leading and trailing meanders of the Polar and Subantarctic Fronts (Hofmann and Whitworth, 1985).

The EOF mode 4 (Fig. 4d) is associated about equally with ML-7 and ML-10 at 500 m. The direction scales on Fig. 4d reflect the fact that flow at the two

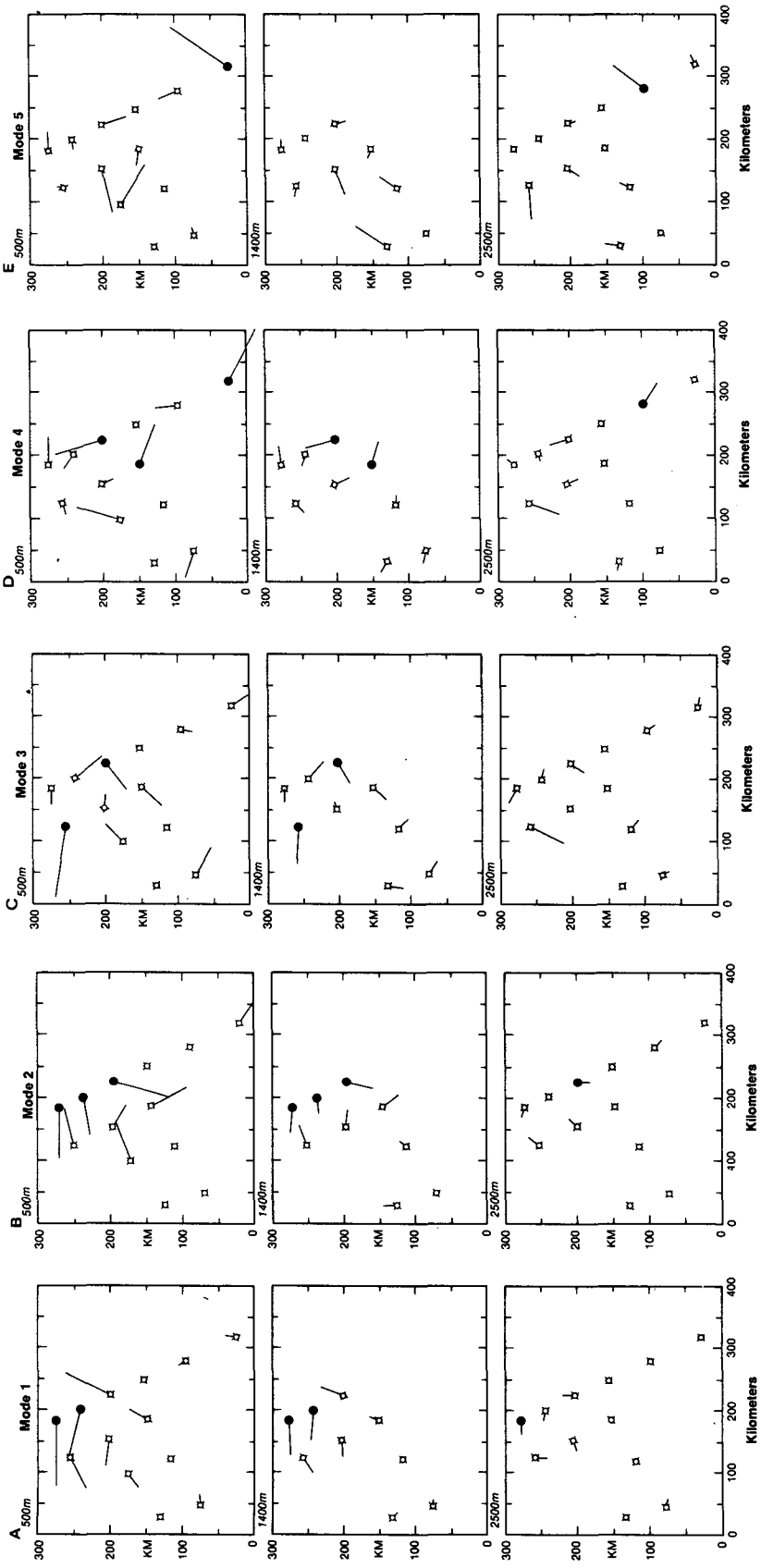

FIG. 5. EOF structures for the five significant modes. The absolute length of the vectors is arbitrary but the relative lengths and directions are meaningful. The vectors with solid markers for moorings explain more than 20% of the residual variance for the given mode. (a) EOF mode 1, (b) EOF mode 2, (c) EOF mode 3, (d) EOF mode 4, (e) EOF mode 5.

meters is nearly in opposite directions. The time series has the ring–meander character seen in modes 2 and 3, with several amplitude maxima of about the same magnitude associated with rotations of the current. This mode is associated with meanders and rings that reach as far south as ML-10. Because of the difference in flow direction (Fig. 5d) the meander is between ML-7 and ML-10.

The last significant EOF mode (Fig. 4e) is related to variability in the southern part of the passage, mainly at ML-10 at 500 m. The most important part of this time series will be those variations that are related to the other EOF modes. This mode will then indicate if the flow at ML-10 is affected by variations at the other locations in the passage. These connections will be indicated through the lagged correlation analysis.

There appears to be some temporal correlation between some of the EOF modes, so rotary coherence was calculated for all possible pairs of time series from the significant EOFs to examine these correlations in the frequency domain. The results were not very satisfying; the rotary autospectra (not shown) for all five amplitude series were red. The resulting coherence calculations gave many random significant (at 99% level) coherence values.

This blurred result occurs for two reasons. There are typically five or fewer "events" in any of the EOF amplitude series, so spectral analysis, which depends on periodic signals, has little information to start with. The second reason is that even if two EOFs appear related, the relative phase of the series changes; that is, they are in phase part of the time and out of phase at other times. Under such circumstances, spectral methods yield little useful information.

To overcome this problem of comparing nonstationary time series, a complex, lagged cross-correlation analysis is performed on pairs of the five significant EOF modes. The determination of significant correlation is taken from Sciremammano (1979). This procedure accounts for the fact that successive observations in a geophysical time series are not statistically independent, and the degrees of freedom for a correlation is not the length of the time series but some smaller value. For this calculation, the degrees of freedom ranged from 20 to 40 which is above the minimum of 10 cited by Sciremammano (1979).

The significant peaks (at an 85% level) for the various calculations are given in Table 4. A positive lag means that the first mode is shifted into the future relative to the second. Because these correlations are for complex (vector) time series, two correlations are possible: inner and outer. Inner correlations compare rotations in the same direction for both time series, while outer correlations are associated with oppositely directed rotations. As an aid to interpreting these results, the amplitude series are compared at significant lags to see if meanders or frontal shifts are causing the correlation. This subjective interpretation is included in the "reason" column of Table 4.

TABLE 4. Significant lagged cross correlations between EOF time series. An inner correlation is between rotations in the same direction, while outer correlations are rotations in opposite directions. The reasons for the correlations are determined subjectively from the time series. The first mode is shifted into the future relative to the second.

Modes	Lag (days)	Type	Reason
1 vs 2	−3	inner	front shift
1 vs 4	+2	outer	front shift
2 vs 3	+16	inner	meanders
2 vs 3	+154	outer	front shift
2 vs 4	+5	outer	meanders
2 vs 4	+147	inner	front shift
2 vs 4	+149	outer	front shift
2 vs 5	+124	outer	front shift
3 vs 4	−9	outer	meanders
3 vs 4	−77	outer	meanders
3 vs 5	−37	outer	meanders
3 vs 5	−99	outer	meanders
4 vs 5	+43	inner	meanders

It is notable that there are no significant autocorrelation peaks, other than the zero lag inner correlation which is not included in the table. After seven to ten days, none of the autocorrelations have significant peaks. Therefore, in spite of the regular variation of the amplitude series (Fig. 4, e.g., 4b), there is no intrinsic regular oscillation of the currents.

The cross correlations do give some information about time scales in the central passage. There appear to be three basic scales: 2–10 days for travel times of mesoscale features, 10–60 days as time between rings or features associated with rings (leading or trailing meanders) and 120–150 days as the time between frontal shifts. These scales are discussed in some detail below.

Two of the correlations involve mode 1 which is mainly the shift of the Polar Front. The correlation between 1 and 2 supports the comments made above that variations due to rings (mode 2) depends on the location of the Polar Front. In other words, the currents from the rings change in different ways depending on whether the Polar Front is near ML-5 or near ML-7. The outer correlation between modes 1 and 4 reflects the fact that the Polar Front shifts between the two moorings. The lag of two days indicates the time required for the shift to occur.

There are three cases where harmonics peaks occur; two of them are 3 versus 4 (outer) and 3 versus 5 (outer). The correlation of 3 versus 4 involves opposite rotations at MS-5 and ML-7, while 3 versus 5 indicates opposite rotations at MS-5 and ML-10. The time span between the peaks is 68 days and 62 days, respectively. This corresponds to the time between rings indicated by mode 2. It is the interplay of

frontal shifts and rings that keeps the autocorrelations from revealing this time scale.

The other harmonic peak occurs in 2 versus 4 (outer) which has a time between peaks of 144 days. There are three other occurrences of correlations at such long lags: 2 versus 3 (outer), 2 versus 4 (inner), 2 versus 5 (inner). An examination of the amplitude series shows that 120 to 150 days is the time between shifts of the Polar Front. This reinforces the fact that the nature of current variation changes as the Polar Front shifts.

One striking result that is evident in Table 3 is that very little of the deep flow is explained by the significant modes—ML-9 at 2500 m is the exception. It may be argued that since EOF modes pick up the largest variance in the data and since the deep flow has smaller variance than the upper flow, then the bottom flow will not have a strong effect on the structure of the modes. The counter-argument is that an EOF mode represents variations from all sensors that have the same time dependence which is determined by the energetic sensors. It appears, therefore, that the deep flow is decoupled from the middle and upper flow.

To analyze this decoupling, an EOF analysis was performed over the deep meters for the same 325 day span used for the whole array. The details of this deep flow analysis will be presented in a following paper but the results are summarized here.

Rotary lagged correlations between amplitude time series for the bottom EOF modes and the whole array EOF modes indicate that there is a correspondence between upper and bottom flow. Most of the significant correlation peaks represent zero lag correlations and 120–150 day correlations. The zero-lag results indicate that the whole array modes contain some information on the lower layer flow. The 120–150 day peaks are due to the strong effect of shifts of the Polar Front which affects every EOF mode to some extent. There is a third group of correlation peaks that indicate that the lower layer may lead the upper layer by a few days. It is this time shift that does not allow the lower layer flow to be represented by the more dominant EOF patterns.

One puzzle from these correlations is that mode 3 (MS-5) always lags any other mode, sometimes by more than 30 days. We know that rings tend to skirt the northern edge of the MS array as they pass through central Drake Passage (Peterson *et al.*, 1982; Hofmann and Whitworth, 1985). However, these studies show that rings are associated with leading and trailing anticyclonic meanders, which interact with the topography of the central passage in an interesting way. The seamount to the west of MS-6 (Fig. 1b) forces the warm meander to the southern side of the MS array while the cold ring moves to the north. The warm meander then affects the southern moorings (MS-7, ML-7) before the ring has a strong effect on MS-5. This conjecture is supported by the correlation analysis (Table 4) that indicates coherent opposite rotations of mode 3 (MS-5) and the southern passage modes (4, 5). The largest delay (other than harmonics) is 37 days which is about half of the estimated time between rings.

The dynamics of this splitting of warm and cold meanders by topography is not clear at this time. It is known (Hofmann and Whitworth, 1985) that some rings tend to "stick" in the central passage for several weeks. It could be that the cold-core rings lodge on the seamount until they separate from the associated warm meander, at which time they propagate northeast through the passage.

If warm and cold features tend to split over this topographic feature then heat flux calculations from these current observations may be much larger than the circumpolar average heat flux. However, there is no way to know if these warm and cold features return to the Polar Front and coalesce as has been observed for Gulf Stream rings, thereby nullifying the measured apparent heat flux. Such questions can not be addressed with this limited measuring program.

4. Summary

This EOF analysis is summarized in the following way. The current associated with the Polar Front has two preferred states: one to the north along MS-5 and ML-5 and another to the south along MS-7 and ML-7. The reason for this behavior appears to be a large seamount just west of MS-6 (Fig. 1b). The two paths are associated with gaps which are the preferred paths for reasons involving conservation of vorticity—rotating flow tends to go around obstacles rather than over them.

The major current variations occur, then, at meters located downstream of the string of seamounts or in the gaps between them. Mooring MS-6 does not participate in this variability because it is too close to the peak of the seamount. At present there is no dynamical argument which gives the size of this shadow zone. The rings and meanders that are prominent in the data seem to skirt the northwestern side of the array. The topography is the likely cause for steering these features northwestward where they can finally move downstream around the topography (Peterson *et al.*, 1982; Hofmann and Whitworth, 1985).

It is curious that MS-1 and MS-3 are not strongly affected by this current variability. There are at least two possible explanations. The rings are produced somewhere upstream and enter this area north of moorings MS-1 and MS-3. They are then steered through the gap at MS-5 to affect the northern current meters. The other possibility is that this variability is generated by flow interaction with the seamounts and there is no variability upstream to detect. Available

information does not allow a choice between these two explanations.

Further studies of the DRAKE 79 data will consider estimates of the terms in the conservation of potential vorticity equation in order to illuminate some of the dynamics involved with these current variations. It may be possible to determine the source of the variability. Also, a dynamic model of this region may determine the importance of the line of seamounts on the baroclinic jet imbedded in the Polar Front. Such modeling work has yet to be attempted.

Acknowledgments. This work was supported by National Science Foundation Grant OCE-8308959.

REFERENCES

Bryden, H. L., 1979: Poleward heat flux and conversion of available potential energy in Drake Passage. *J. Mar. Res.*, **37**, 1–22.

Denbow, D. W., and J. S. Allen, 1984: Rotary empirical orthogonal function analysis of currents near the Oregon Coast. *J. Phys. Oceanogr.*, **14**, 35–46.

Hardy, D. M., 1977: Empirical eigenvector analysis of vector observations. *Geophys. Res. Lett.*, **4**, 319–320.

——, and J. J. Walton, 1978: Principle component analysis of vector wind measurements. *J. Appl. Meteor.*, **17**, 1153–1162.

Hofmann, E. H., and T. Whitworth III, 1985: A synoptic description of the flow at Drake Passage from year-long measurements. *J. Geophys. Res.*, (in press).

Inoue, M., 1982: Vertical structure of low-frequency currents at Drake Passage. Ph.D. dissertation. Texas A&M University, 220 pp.

Joyce, T. M., and S. L. Patterson, 1977: Cyclonic ring formation of the Polar Front Zone in the Drake Passage. *Nature*, **265**, 131–133.

——, —— and R. C. Millard, Jr., 1981: Anatomy of a cyclonic ring in the Drake Passage. *Deep-Sea Res.*, **28A**, 1265–1287.

Legeckis, R., 1977: Oceanic polar front in the Drake Passage—satellite observations during 1976. *Deep-Sea Res.*, **24**, 701–704.

Legler, D. M., 1983: Empirical orthogonal function analysis of wind vectors over the tropical Pacific region. *Bull. Amer. Meteor. Soc.*, **64**, 234–241.

Nowlin, W. D., Jr., T. Whitworth III and R. D. Pillsbury, 1977: Structure and transport of the Antarctic Circumpolar Current at Drake Passage from short term measurements. *J. Phys. Oceanogr.*, **7**, 787–802.

——, and M. A. Clifford, 1982: The kinetic and thermohaline zonation of the ACC at Drake Passage. *J. Mar. Res.*, **40**(Suppl.), 481–507.

Peterson, R. G., W. D. Nowlin, Jr. and T. Whitworth III, 1982: Generation and evolution of a cyclonic ring at Drake Passage in early 1979. *J. Phys. Oceanogr.*, **12**, 712–719.

Pillsbury, R. D., J. S. Bottero and R. E. Still, 1981: A compilation of observations from moored current meters. Vol. 14. Current, temperature and pressure in the Drake Passage during DRAKE 79, January 1979–January 1980, Part A and B, School of Oceanography, Oregon State University, Data Rep. 91, Ref. 91-17, A: 373 pp.; B: 215 pp.

Priesendorfer, R. W., F W. Zwiers and T. P. Barnett, 1981: Foundations of principal component selection rules. SIO Ref. Ser. 81-4, Scripps Institution of Oceanography, La Jolla, Ca. 192 pp.

Reid, J. L., and W. D. Nowlin, Jr., 1971: Transport of water through the Drake Passage. *Deep Sea Res.*, **18**, 51–64.

Sciremammano, F., Jr., 1979: A suggestion for the presentation of correlations and their significance levels. *J. Phys. Oceanogr.*, **9**, 1273–1276.

——, R. D. Pillsbury, W. D. Nowlin, Jr. and T. Whitworth, III, 1980: Spatial scales of temperature and flow in Drake Passage. *J. Geophys. Res.*, **85**, 4015–4028.

Whitworth, T. III, 1980: Zonation and geostrophic flow of the Antarctic Circumpolar Current at Drake Passage. *Deep-Sea Res.*, **27**, 497–507.

——, 1983: Monitoring the transport of the Antarctic Circumpolar Current at Drake Passage. *J. Phys. Oceanogr.*, **13**, 2045–2057.